Electrochimica Acta 174 (2015) 945–954

Contents lists available at ScienceDirect

Electrochimica Acta

journal homepage: www.elsevier.com/locate/electacta

Multi-physics Model for the Aging Prediction of a Vanadium Redox Flow Battery System

Ghada Merei[a,b,c,*], Sophie Adler[a], Dirk Magnor[a,b,c], Dirk Uwe Sauer[a,b,c]

[a] Electrochemical Energy Conversion and Storage Systems Group, Institute for Power Electronics and Electrical Drives (ISEA), RWTH Aachen University, Germany
[b] Juelich Aachen Research Alliance, JARA-Energy, Germany
[c] Institute for Power Generation and Storage Systems (PGS), E.ON ERC, RWTH Aachen University, Germany, Jaegerstrasse 17-19, 52066 Aachen Germany

ARTICLE INFO

Article history:
Received 11 May 2015
Received in revised form 9 June 2015
Accepted 15 June 2015
Available online 25 June 2015

Keywords:
redox-flow battery
multi-physics model
side reactions
Matlab/Simulink

ABSTRACT

The all-vanadium redox-flow battery is an attractive candidate to compensate the fluctuations of non-dispatchable renewable energy generation. While several models for vanadium redox batteries have been described yet, no model has been published, which is adequate for the aging prediction. Therefore, the present paper presents a multi-physics model which determines all parameters that are essential for an aging prediction. In a following paper, the corresponding aging model of vanadium redox flow battery (VRB) is described. The model combines existing models for the mechanical losses and temperature development with new approaches for the batteries side reactions. The model was implemented in Matlab/Simulink. The modeling results presented in the paper prove to be consistent with the experimental results of other research groups.

© 2015 Elsevier Ltd. All rights reserved.

1. Introduction

With the rapid growth of renewable energy generation, large energy storage systems are promising solutions to compensate for the fluctuations of non-dispatchable renewable energy generation [1]. The all-vanadium redox-flow battery (VRB) is an attractive candidate to provide this compensation due to its long lifetimes, its fast-response, high energy efficiencies and the possibility of independent scale-up of nominal power and nominal energy [2].

VRB systems are electrochemical systems which utilize the same element in both half-cells. This avoids cross-contamination. VRB systems operate with V^{2+} and V^{3+} as a redox couple in the negative half-cell and the redox couple VO^{2+}/VO_2^+ (V^{5+}/V^{4+}) in the positive half-cell [3]. They consist of two reservoirs which contain the electrolytes with the redox couples V^{2+}/V^{3+} and VO^{2+}/VO_2^+ (Fig. 1). From the two reservoirs, the electrolytes are circulated through the stack using two pumps in order to enable the electrochemical reactions at the cells' inert electrodes [3]:

$$V^{2+} \rightleftarrows V^{3+} + e^- (\text{negative half} - \text{cell})$$

$$VO_2^+ + 2H^+ + e^- \rightleftarrows VO^{2+} + H_2O (\text{positive half} - \text{cell})$$

The cells are usually connected in series. Thus, a serial connection is assumed in the equations in Section 2.

In each cell, an ion-exchange membrane limits the cross-mixing of these electrolyte solutions, but allows for the diffusion of H^+ ions [3].

Aging prediction is essential to estimate the overall lifetime costs of a battery system. While several models for vanadium redox batteries have been described yet, no model has been published, which is adequate for the aging prediction of a vanadium redox flow battery. Therefore, the current paper presents a multi-physics model which determines all parameters that are essential for an aging prediction. This includes the battery's state of charge (SOC), the stack and tank temperature, the corrosion current and the V (IV) and V(V) concentrations in the reservoirs. In the following paper, the corresponding VRB aging model is described.

The model combines existing models for the mechanical losses and temperature development with new approaches for the battery's side reactions. It was implemented in Matlab Simulink.

2. The Multi-physics model

The multi-physics VRB model (Fig. 2) takes into account the temperature changes in the VRB during charging and discharging (*Temperature model*), the main electrochemical reactions and the side reactions H_2 evolution, O_2 evolution and vanadium diffusion through the membrane (*Electrochemical model*) as well as the

* Corresponding author.

http://dx.doi.org/10.1016/j.electacta.2015.06.046
0013-4686/© 2015 Elsevier Ltd. All rights reserved.

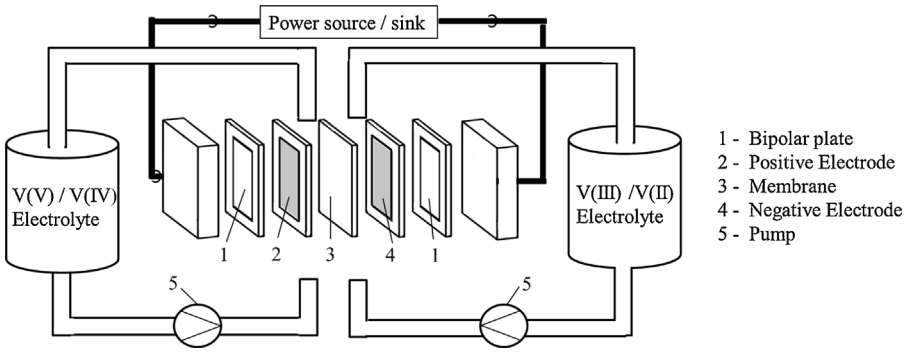

Fig. 1. Schematic set-up of a vanadium redox flow battery system.

pump losses within the VRB system (*Mechanical Model*). Moreover, it considers the battery's characteristics (nominal power and capacity, battery design and electrolyte compositions), voltage and SOC limits, the temperature of the environment T_{air} and the battery system power P_{VRB} are used as input parameters.

During charging, the battery system power P_{VRB} is delivered to the battery by an external charger. The battery system power splits up into the power losses for pumping the electrolyte P_{pump}, the power losses for the heating or cooling system (in case heating or cooling is needed) $P_{Heating/cooling}$, the power P_{charge} which is charged to the battery. During discharging, the discharging power $P_{discharge}$ provides for the power losses and the battery system power P_{VRB} which is delivered from the battery system to an external load. An overview on the different parameters and the values assumed for the simulation is given in Table 1.

I. Mechanical Model

The mechanical model determines the pump power required to let the electrolyte flow from the tanks through the stack and back. The implemented model is based on the approach presented in [4] and takes into account both the mechanical losses in the pipes, bends, valves, pumps and tanks and the mechanical losses in the stack. It is applicable for VRBs with different sizes, designs and electrolyte concentrations [4].

The pumping losses of the two pumps P_{pump} can be determined using the flowrate Q $[m^3/s]$ and the pressure drop across the hydraulic system Δp_{system} [5]:

$$P_{pump} = 2 \cdot \frac{1}{\eta_{pump}} \cdot \Delta p_{system} \cdot Q[W] \quad (1)$$

where η_{pump} is the pump efficiency, Q is the electrolyte flow rate in $[m^3/s]$.

The flow rate of the electrolyte Q is determined based on Faraday's law of electrolysis:

$$Q = \frac{2 \cdot N_{cell} \cdot |I_{stack}(t)|}{n \cdot F \cdot c_{Vanadium} \cdot SOC_{min}} \left[\frac{m^3}{s}\right] \quad (2)$$

where N_{cell} is the number of cells, $I_{stack}(t)$ is the stack current, n is the number of electrons transferred during the redox reaction which is 1 for the VRB, F is the Faraday constant, $c_{Vanadium}$ is the total vanadium concentration of each tank and SOC_{min} is the minimum state-of charge.

The pressure drop Δp_{system} can be modeled as the sum of the pressure drop in the stack Δp_{stack} and in the pipes Δp_{pipe} [6]. The pressure drop Δp_{stack} in the stack is modeled using an analogy of Ohm's law [4]:

$$\Delta p_{stack} = Q \cdot \tilde{R}[Pa] \quad (3)$$

where $\tilde{R}$ is the hydraulic resistance in $[Pa \cdot s/m^3]$. The hydraulic resistance can be obtained by decomposing the stack into smaller parts for which estimations of the hydraulic resistance $\tilde{R}_i$ are available in [4]. These hydraulic resistances of the components can then be combined to determine the hydraulic resistance of a stack of any size [4]. This method can only be used if the flow in the stack stays laminar. Blanc has demonstrated that this assumption is valid even at a maximal flow rates [4].

The pressure drop in the pipes Δp_{pipe} can be determined using an extended Bernoulli equation. This takes into account the losses due to the change in electrolyte velocity $h_{\Delta v_s}$ in [m], the losses due to the change in height Δz in [m], due to the head losses h_f because of friction in the straight sections of the pipe in [m] and minor losses in the bends and valves h_m in [m] [5]:

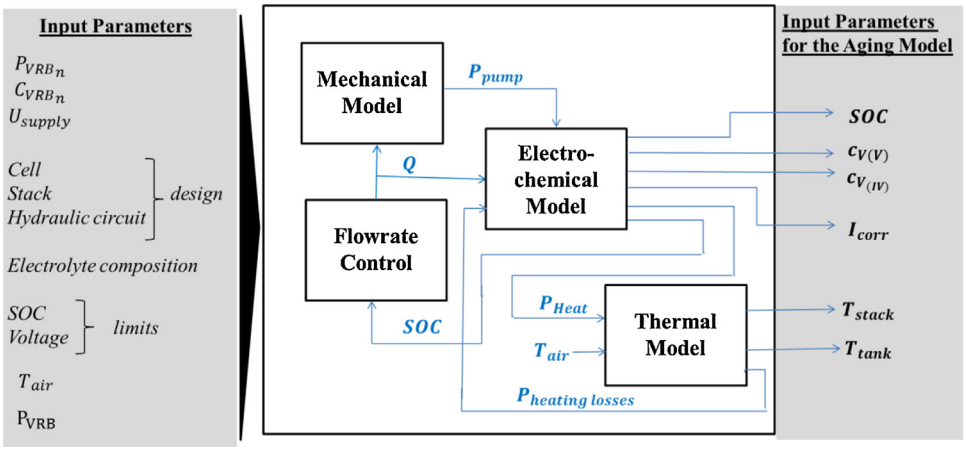

Fig. 2. Overview on the multi-physics VRB model.

$$\Delta p_{\text{pipes}} = \gamma \cdot (h_{\Delta v_s} + \Delta z + h_f + h_m)[\text{Pa}]$$

In the Bernoulli equation, γ is the specific weight in $[\text{N/m}^3]$. The head losses h_f and the minor losses h_m can be calculated using the Darcy–Weißbach equation (c.f. [4]).

Velocity change losses occur when the electrolyte flows from the tanks to the pipes (sudden contraction) and reenters the tanks again (sudden expansion). The velocity change due to the electrolyte's entering and leaving the stack is included in the stack losses. Thus, the velocity change losses are determined using the following equation [4]:

$$h_{\Delta V_s} = \frac{v_{s,\text{expansion}}^2}{2 \cdot g} \cdot \left(1 - \frac{A_{\text{pipes}}}{A_{\text{tank}}}\right)^2 + \frac{v_{s,\text{contraction}}^2}{2 \cdot g} \cdot k_{L_{\text{contraction}}}[\text{m}] \quad (5)$$

Where $v_{s,\text{expansion}}^2$ and $v_{s,\text{contraction}}^2$ are the velocities of the electrolytes in the pipes before the sudden expansion or and after the sudden contraction in $[\text{m/s}]$,g is the gravitational acceleration in $[\text{m/s}^2]$, A_{pipes} is the cross area of the pipes in $[\text{m}^2]$, A_{tank} is the cross area of the tank inlet in $[\text{m}^2]$ and $k_{L_{\text{contraction}}}$ is the dimensionless loss coefficient which depends on the geometry of the entrance region (c.f. [4]).

II. Electrochemical Model

The electrochemical model determines the VRB's state of charge which includes the calculation of the vanadium concentrations in both tanks, the operational voltage, the corrosion current and the V(IV) and V(V)-concentration which are needed for the aging prediction.

The stack voltage can be described by the equilibrium voltage E_{Eq} [V] and the sum of overpotentials:

$$U_{\text{stack}} = N_{\text{cell}} \cdot (E_{\text{eq}} - \eta_{\text{act}} - \eta_{\text{conc}} - \eta_{\text{ohm}} - \eta_{\text{ionic}})[\text{V}] \quad (6)$$

Where N_{Cell} is the number of cells per stack that are connected in series, η_{act} is the activation overpotential, η_{conc} is the concentration overpotential and η_{ohm} and η_{ionic} are the ohmic overpotential associated with the ohmic losses in the electrodes, plates and wires and the ionic overpotential due to the ionic losses in the electrolytes and membranes respectively.

The equilibrium potential E_{eq} is calculated using the Nernst equation [4]:

$$E_{eq} = E^{\theta'} + \frac{R \cdot T_s}{n \cdot F} \cdot \ln\left\{\left(\frac{c_{V(V)} \cdot c_{H^+}^2}{c_{V(IV)}}\right)_{\text{catholyte}} \cdot \left(\frac{c_{V(II)}}{c_{V(II)}}\right)_{\text{anolyte}}\right\}[\text{V}] \quad (7)$$

Where $E^{\theta'}$ is the standard potential[V] for a full charge battery with V(II) und V(V) concentrations of one mole/l, R is the universal gas constant [J/mol·K], T_s the stack temperature in [K], n is number of electrons in the reaction which is one for the VRB reaction, F is the Faraday constant in [A · s/mol] and c_i is the concentration in [mol/L] of the respective vanadium species or hydrogen. The concentration $c_{V(V)}$ and $c_{V(IV)}$ are the concentrations of VO_2^+ and VO^{2+} respectively. The formal potential $E^{\theta'}$ can be replaced by the standard potential E^{θ} if the effect of the activity coefficients γ_i of the different species (vanadium species and hydrogen) is considered to cancel each other approximately [4].

The activation potential η_{act} can be calculated by inverting the Butler–Volmer equation if the mass transfer effects are negligible [4]:

$$I = I_0 \cdot \left(e^{\frac{\alpha \cdot \eta \cdot \eta_{\text{act}}}{RT_s}} - e^{-\left(\frac{(1-\alpha) \cdot \eta_{\text{act}}}{RT_s}\right)}\right) \quad (8)$$

Where R is the ideal gas constant, T_s is the stack temperature in Kelvin, n is the number of moles exchanged in the reaction which is one for the VRB reaction, α is the charge transfer coefficient and I_0 is the exchange current. The exchange current I_0 is the magnitude of the partial anodic and partial cathodic currents which are equal at equilibrium [7]. They can be calculated based on the exchange current densities i_1^0 and i_2^0 [8]:

$$i_1^0 = F \cdot k_1^{\theta} \cdot (c_{V(II)})^{\alpha_{1,c}} \cdot (c_{V(III)})^{\alpha_{1,c}}\left[\frac{\text{A}}{\text{m}^2}\right] \quad (9)$$

$$i_2^0 = F \cdot k_2^{\theta} \cdot (c_{V(IV)})^{\alpha_{2,c}} \cdot (c_{V(V)})^{\alpha_{2,\alpha}}\left[\frac{\text{A}}{\text{m}^2}\right] \quad (10)$$

where i_1^0 and i_2^0 are the exchange current densities in $[\text{A/m}^2]$, ${k_1}^{\theta}$ and ${k_2}^{\theta}$ are the reaction constants for the reactions at the positive and negative electrode in [m/s], c_i are the concentrations of the different vanadium species in [mol/1] and α_i are the dimensionless charge transfer coefficients. The reaction rates can then be calculated [9]:

$${k_1}^{\theta} = {k_{1,\text{ref}}}^{\theta} \cdot \exp\left(-\frac{FE_1^{\theta}(T_{\text{ref}})}{R} \cdot \left(\frac{1}{T_{\text{ref}}} - \frac{1}{T_s}\right)\right)\left[\frac{\text{m}}{\text{s}}\right] \quad (11)$$

$$k_2^{\theta} = {k_{2,\text{ref}}}^{\theta} \cdot \exp\left(\frac{FE_2^{\theta}(T_{\text{ref}})}{R} \cdot \left(\frac{1}{T_{\text{ref}}} - \frac{1}{T_s}\right)\right)\left[\frac{\text{m}}{\text{s}}\right] \quad (12)$$

where E_1^{θ} and ${E_2}^{\theta}$ are the reference potentials for the reactions at both electrodes [V], $k_{1,\text{ref}}\theta$ and $k_{2,\text{ref}}\theta$ are the rates of constants in [m/s] at a reference temperature T_{ref} [K], T_s is the stack temperature [K].

The concentration overpotential η_{conc} caused by the concentration difference between the bulk solution and the electrode surface can be determined using the following equation [4]:

$$\eta_{\text{conc}} = \frac{R \cdot T_s}{F} \times \ln\left(\frac{c_{V(V)}(\infty) \cdot c_H^+(\infty)^2 \cdot c_{V(II)}(\infty)}{c_{V(IV)}(\infty) \cdot c_{V(III)}(\infty)} \cdot \frac{c_{V(IV)}(0) \cdot c_{V(III)}(0)}{c_{V(V)}(0) \cdot c_H^+(0)^2 \cdot c_{V(II)}(0)}\right)[V] \quad (13)$$

The ohmic and ionic overpotentials η_{ohm} and η_{ionic} can be determined based on the equivalent cell area resistivity $R_{\text{c,area}}$ $[\Omega/\text{m}^2]$, which differs during charging and discharging.

As vanadium diffusion through the membrane can occur, the state of charge is determined as the minimum of the vanadium concentrations in the two half-cells:

$$SOC = \min\left(\left(\frac{c_{V(II)}}{c_{V(II)} + c_{V(III)}}\right), \left(\frac{c_{V(V)}}{c_{V(IV)} + c_{V(V)}}\right)\right)[-] \quad (14)$$

where c_{V_i} are the concentrations of the different vanadium species in [mol/L].

The stack current splits up into three components: the charging or discharging current ($I_{c/d}$) [A] controlling the main reaction, the corrosion current I_{corr} [A] and the hydrogen evolution current I_h [A]:

$$I_{\text{stack}} = I_{c/d} + I_{\text{corr}} + I_{H_2}[\text{A}] \quad (15)$$

Vanadium Cross-over

The battery's SOC depends on the concentration of the different vanadium species in the positive and negative half-cell. The vanadium concentration changes due to the charging and discharging reaction and due to vanadium diffusion through the membrane. The model for Vanadium diffusion is based on [10] and takes into account two reactions in the positive and two reactions in the negative half cell:Table 2 Cross-over reactions in the positive and negative half-cell

Table 1
Overview on the main input parameters for the VRB model.

Parameter	Description	Value	
P_r	Power rating [W]	5100	Fig. 2
C_r	Faradic capacity [Ah]	1600	Fig. 2
U_{supply}	Supply voltage [V]	48	Fig. 2
η_{pump}	Pump efficiency [%]	85	Eq. (1)
N_{cell}	Number of cells	39	Eq. (2)
$c_{H_2SO_4}$	Sulfuric acid concentration per tank [M/1]	3	
$c_{vanadium}$	Vanadium concentration per tank [M/1]	1.6	Eq. (2)
SOC_{min}	Minimal SOC [%]	5	Eq. (2)
SOC_{max}	Maximal SOC [%]	100	
$\tilde{R}$	Hydraulic resistance of the stack $[\frac{Pa \cdot s}{m^3}]$	4 844 764	Eq. (2)
Δz	Difference in height [m]	0	Eq. (4)
γ	Specific weight [Nm^{-3}]	1588.7	Eq. (4)
$k_{L_{contraction}}$	Entrance loss coefficient [–]	0.5	Eq. (5)
A_{pipes}	The area of the pipes [m^2]	0.3142	Eq. (5)
A_{tank}	Entrance area of each tank [m^2]	0.7163	Eq. (5)
L_{pipe}	Total length of each pipe [m]	4.46	
D_{pipe}	Pipe diameter [m]	0.02	
η_{conc}	Concentration overpotential	0	Eq. (6)
E_1^{θ}	Reference potential for first reaction [V]	-0.26	Eq. (11)
$k_{1,ref^{\theta}}$	Reference rate constant for first reaction at 293 K [ms^{-1}]	3.56×10^{-6}	Eq. (11)
T_{ref}	Reference temperature for reaction rate calculation [K]	293	Eq. (11)
E_2^{θ}	Reference potential for second reaction [V]	1.004	Eq. (12)
$k_{2,ref^{\theta}}$	Reference rate constant for first reaction at 293 K [ms^{-1}]	3×10^{-9}	Eq. (12)
V_h	Volume of one half-cell electrolyte [1]	0.9	Eq. (16)
$A_{electrode}$	Electrode area per cell [m^2]	0.22	Eq. (16)
$d_{membrane}$	Thickness of the membrane [m]	0.0012	Eq. (16)
S	Membrane area [m]	21.99	Eq. (16)
$E_{2,SCE}^{\theta}$	Standard reduction potential of the positive electrode vs. SCE [V]	0.7630	Eq. (23)
V_{tank}	Electrolyte volume per tank [1]	1757.1	Eq. (24)
V_{stack}	Stack volume [1]	35.1	Eq. (24)
UA	Heat transfer through the tank wall [WK^{-1}] [1]	37.92	Eq. (24)
R_c	Charging average cell resistivity [Ωcm^2] [4]	2.9	Eq. (25)
R_d	Discharging average cell resistivity [Ωcm^2] [4]	3.13	Eq. (25)
ρ	Density [kgm^{-3}]	1620	Eq. (25)
T_{min}	Lower temperature limit of the battery [K]	283.15	Eq. (26)
$t_{timestep}$	Length of one timestep [s]	600	Eq. (26)
T_{max}	Upper temperature limit of the battery [K]	313.15	Eq. (27)
μ	Viscosity [Pa/s]	0.008	
$k_{L,minor}$	Hydraulic loss coefficient for minor losses	1.05	
$\alpha_{1,\alpha}, \alpha_{2,\alpha}$	Anodic transfer coefficients: positive & negative	0.5	
$\alpha_{1,c}, \alpha_{2,c}$	Cathodic transfer coefficients: positive & negative	0.5	
θ	Polypropylene thickness of the tank [m] [1]	0.01	
k	Polypropylene conductivity of the tank [$Wm^{-1}K-1$] [1]	0.16	

Tang et al. based their model on six assumptions:

1. The flow of the electrolyte is not taken into account.
2. The side reactions due to diffusion are instantaneously.
3. The volumes of both half-cell electrolytes remain constant.
4. The rates of self-discharge reactions can be described by Faraday's law of electrolysis.
5. The electrolytes are perfectly mixed.
6. The proton concentration remains constant during charge-discharge cycling.
7. The bulk electrolyte transfer through the membrane which results in a change of volume in each half cell [11], has not been considered.

Table 2
Cross-over reactions in the positive and negative half-cell.

Reactions in the positive half-cell	Reactions in the negative half-cell
$V^{2+} + 2V^{5+} \Rightarrow 3V^{4+}$	$V^{5+} + 2V^{2+} \Rightarrow 3V^{3+}$
$V^{3+} + V^{5+} \Rightarrow 2V^{4+}$	$V^{4+} + V^{2+} \Rightarrow 2V^{3+}$
$V^{2+} + V^{4+} \Rightarrow 2V^{3+}$	$V^{5+} + V^{3+} \Rightarrow 2V^{4+}$

Based on these assumptions and molar mass balance, the concentration change due to vanadium ion diffusion can be described by the following dynamic equations [10]:

$$\frac{dc_{V_j}}{dt}(t,T) = \left(\pm\frac{i_{c/d} \cdot A_{\text{Electrode}}}{F} - \frac{\alpha_{IIj} \cdot k_2(T_s) \cdot c_{V(II)} \cdot S}{d_{\text{Membrane}}} - \frac{\alpha_{IIIj} \cdot k_3(T_s) \cdot c_{V(III)} \cdot S}{d_{\text{Membrane}}}\right) - \frac{\alpha_{IVj} \cdot k_4(T_s) \cdot c_{V(IV)} \cdot S}{d_{\text{Membrane}}} - \frac{\alpha_{Vj} \cdot k_5(T_s) \cdot c_{V(II)} \cdot S}{d_{\text{Membrane}}} \cdot \frac{1}{V_h}\left[\frac{\text{mol}}{\text{m}^3}\right] \quad (16)$$

where c_{V_j} with $j = II..V$ are the concentrations of the vanadium species in $[\text{mol}/1]$, k_2, k_3, k_4, k_5 are the temperature dependent diffusion coefficients of the different vanadium species in $[\text{m}^2/\text{s}]$, α_{j_i} are ratio coefficients summarized in Table 3, V_h is the volume of one half-cell solution [L], $i_{c/d}$ is the charging or discharging current density in [A/cm], A is the electrode surface area in [cm^2], d_{Membrane}

Table 3
Coefficients reflecting the diffusion of the different vanadium species [14].

i	α_{II_i}	α_{III_i}	α_{IV_i}	α_{V_i}
$V(II)$	1	0	1	2
$V(III)$	0	1	-2	-3
$V(IV)$	-3	-2	1	0
$V(V)$	2	1	0	1

is the thickness of the membrane in [dm] and S is the membrane area in [dm^2]. The signs '+' and '−' stand for the process of charging and discharging.

Hydrogen Evolution Current

The oxygen and hydrogen evolution in electrode compartments lead to imbalanced in capacity losses of the positive and negative half-cell. In this paper the oxygen evolution is not considered since it can be neglected up to high SOC. Hydrogen evolution is included in the model since it can be "quite significant above 90% SOC" and it consumes a portion of current applied to the cell [10]. A new approach is chosen which is based on data measurements. This approach models hydrogen evolution as a function of the negative electrode potential, but does not take into account effects such as the reduced transport coefficients or active surface due to gas bubbles.

The model determines the hydrogen evolution current I_{H_2} based on the coulombic efficiency $\eta_{V(III)-V(II)}$, which is a function of the polarization potential, the sulfuric acid concentration and V(III) concentration:

$$I_{H_2} = \left(1 - \eta_{V(III)-V(II)}\right) \cdot I_{V(III)-V(II)}[A] \tag{17}$$

In this equation, $I_{V(III)-V(II)}$ is the current for the conversion of V(III) to V(II) during charging which is equal to I_c. The coulombic efficiency $\eta_{V(III)-V(II)}$ at different polarization potentials, sulfuric acid and V(III) concentrations can be determined using the data from a systematic investigation published in [12].

Corrosion Current

The corrosion current evolving at the positive electrode during charging is taken into account in order to set the right voltage limits to prevent corrosion. The corrosion current model is based on measurements of the corrosion current density for different temperatures, polarization times and polarization potentials, which are published in [13], and on measurements of the increase in internal resistance due to introduction of functional groups of COOH and C=O in the surface of the electrode which occur during the corrosion process. These measurements are published in [14]. These demonstrate that the corrosion current density increases linearly with polarization time until it reaches its maximum value. The corrosion current starts to flow once a specific polarization potential—the initial corrosion potential is reached.

$$i_{corr}(t_{pol}, E_{initial}, E^+_{SCE}) = \begin{cases} 0, for t_{pol} \le 0 \cup E^+_{SCE} < E_{initial} \\ i_{corr,initial} + t_{pol} \cdot \left(\frac{i_{corr,max} - i_{corr,initial}}{t_{pol,max}}\right), for 0 < t_{pol} < t_{pol,max} \cap E^+_{SCE} \ge E_{initial} \\ i_{corr,max}, for t_{pol} \ge t_{pol,max} \cap E^+_{SCE} \ge E_{initial} \end{cases} \tag{18}$$

where t_{pol} is the polarization time [s], $E_{initial}$ is the initial corrosion potential [V], E^+_{SCE} is the positive electrode potential, $i_{corr,initial}$ is the initial corrosion current density (the corrosion current density in the moment in which the corrosion process starts) [A/m^2], $i_{corr,max}$ is the maximum value of the corrosion current density and $t_{pol,max}$ is the polarization time [s], after which the maximum value of the corrosion current density is reached.

Below this initital corrosion potential, the current flows due to the electrochemical oxidation of VO^{2+} and thus, is independent from polarization time. Above the intial corrosion potential, the current density is partly due to the electrochemical oxidation and partly due to corrosion. The corrosion current density can be calculated by subtracting the amount of current density for the electrochemical oxidation of VO^{2+} from the entire current density [13]. Therefore, the corrosion current density can be described by the equation 18.

Values for the initial corrosion potential $E_{initial}$ [V] are taken from the measurements in [13]. The initial corrosion current density $i_{corr,initial}$, its maximum value $i_{corr,max}$ and time $t_{pol,max}$ is estimated using the following equations. These are based on the change of these parameters with E_{pol} which is estimated based on the measurements in [13]:

$$i_{corr,initial} = 0.025\frac{A}{cm^2} \cdot 2^{\frac{E^+_{SCE} - 1.75V}{0.05V}} \quad \left[\frac{A}{cm^2}\right] \tag{19}$$

$$i_{corr,max} = 0.144\frac{A}{cm^2} \cdot 1.125^{\frac{E^+_{SCE} - 1.75V}{0.05V}} \quad \left[\frac{A}{cm^2}\right] \tag{20}$$

$$t_{pol,max} = 7200s \cdot 2^{\frac{E^+_{SCE} - 1.75V}{0.05V}}[s] \tag{21}$$

The positive electrode potential E^+_{SCE} against the saturated calomel electrode (SCE) is determined based on the open circuit potential at the positive electrode E^+_{eq} [V] the activation potential η^+_{act} [V], the stack current I_{stack} [A] and the cell resistance R_{cell} [Ω]:

$$E^+_{SCE} = E^+_{eq} + \eta^+_{act} + \frac{1}{2} \cdot R_{cell} \cdot I_{stack}[V] \tag{22}$$

R_{cell} is the product of R_c or R_d, the electrode area $A_{Electrode}$.It is assumed that the contribution of the losses is equally distributed between the positive and the negative electrode. The open circuit potential can be estimated using the Nernst equation [8]:

$$E^+_{eq} = E^{\theta}_{2,SCE} + \frac{RT_s}{F} \cdot \ln\left(\frac{c_V}{c_{IV}}\right)[V] \tag{23}$$

where $E^{\theta}_{2,SCE}$ is the standard reduction potential of the positive electrode versus saturated calomel electrode (SCE). The positive activation potential is calculated using equation (8).

III. Temperature Model

The thermal model predicts the stack and tank temperature (T_s and T_t respectively) as functions of current, ambient temperature and flow rate. The model is implemented as a state-space model since numerical procedures such as the Euler integration method did not deliver accurate results for time steps of 10 minutes or above.

The change of the stack and tank temperature can be derived from the law of energy conservation [1]:

$$\begin{bmatrix} \frac{dT_s}{dt} \\ \frac{dT_t}{dt} \end{bmatrix} = \begin{bmatrix} -\frac{Q}{V_{stack}} \cdot 2 & \frac{Q}{V_{stack}} \cdot 2 \\ \frac{Q}{V_{tank}} & -\frac{Q}{V_{tank}} - \frac{UA}{C_p \cdot \rho \cdot V_{tank}} \end{bmatrix} \begin{bmatrix} T_s \\ T_t \end{bmatrix} + \beta \left[\frac{K}{s}\right] \quad (24)$$

Where V_{stack} is the volume of the stack [m^3], C_p is the heat capacity of the electrolyte [$JK^{-1}kg^{-1}$], ρ is the electrolyte density [kgm^{-3}], V_{tank} is the volume of one VRB tank [m^3] and UA is the heat transfer through the tank wall [WK^{-1}]. It is assumed that the flow rate of the positive and negative electrolyte is equal ($Q = Q_+ = Q_-$) as are the temperatures in the tanks on the positive and negative side ($T_t = T_+ = T_-$), the volumes of the tanks ($V_t = V_+ = V_-$) and the heat transfer of the tanks ($U_-A_- = U_+A_+$). The heat capacity C_p[$JK^{-1}kg^{-1}$] is calculated each time step based on the group distribution method and data taken from [14–18].

The vector β is a vector of the temperature changes due to heat generation during the operation of the battery ($I_{stack}{}^2 \cdot R_{stack}$), cooling through temperature exchange with the surrounding air ($T_{air} \cdot UA$) and the heating and cooling via a combined heating-and-cooling system:

$$\beta = \begin{bmatrix} \frac{U_{stack} - U_{equilibrium}}{C_p \cdot \rho \cdot V_{stack}} \\ UA \times \frac{T_{air}}{C_p \cdot \rho \cdot V_{tank}} + \frac{1}{C_p \cdot \rho \cdot V_{tank}} (P_{heating} - P_{cooling}) \end{bmatrix} \left[\frac{K}{s}\right] \quad (25)$$

With

Where $P_{heating}$ and $P_{cooling}$ are the powers used for the heating and cooling of the battery (if a cooling or heating system exists), I_{stack} is the stack current [A], R_{stack} is the stack resistance which is the product of R_c or R_d, the electrode area $A_{Electrode}$ and the number of cells N_{cell}[Ω], T_{air} is the temperature of the surrounding air [K], T_{min} is the minimum temperature of the VRB (usually around 10 °C) in [K], $t_{timestep}$ is the length of one time step [s] and T_{max} is the maximum temperature of the VRB (usually around 40 °C) in [K]. The heating and cooling powers $P_{heating}$ and $P_{cooling}$ are not equivalent to the electric power losses of the heating and cooling system $P_{heating\ losses}$, but depend on the coefficient of performance of the heating or cooling system ε_{w_i}.

$$P_{cooling} = \left\{ C_p \cdot \rho \cdot V_{tank} \cdot \frac{T_{max} - T_t}{t_{timestep}} - \frac{Q}{V_{tank}} \cdot (T_t - T_s) - \frac{UA}{C_p \cdot \rho \cdot V_{tank}} \cdot (T_{air} - T_t) + I_{stack}^2 \cdot R_{stack} if T_s < T_{max} \right[W]0 if T_s \geq T_{max} \quad (26)$$

$$P_{heating} = \left\{ C_p \cdot \rho \cdot V_{tank} \cdot \frac{T_{min} - T_t}{t_{timestep}} - \frac{Q}{V_{tank}} \cdot (T_t - T_s) - \frac{UA}{C_p \cdot \rho \cdot V_{tank}} \cdot (T_{air} - T_t) if T_t < T_{min} \right[W]0 if T_t \geq T_{min} \quad (27)$$

It is to be mentioned that the pump power converts to heat through the friction of the electrolyte and the wall of the path [19]. However, this heat term has not been considered in the current work. In the future work about predicting the battery aging, this term will be taken into account.

3. Simulation of the Multi-physics Model

In order to prove consistency with the experimental results of other research groups, the multi-physics VRB model was simulated over a period of about four days. The vanadium redox flow model is integrated into a model for an off-grid PV- wind- diesel battery hybrid system to supply the energy to a 3 kW telecommunication base station. Detailed information about the system can be found in [20].

I. Battery characteristics

To prove that the model is working properly, the next two figures are illustrated. Fig. 3 shows the charging/discharging processes using different currents. It is to be noticed that the high currents cause faster charging and discharging. At smaller currents, the battery takes longer time to be fully charged or discharged.

Furthermore, the battery characteristics are illustrated in the following figure (Fig. 4). The figure shows the state of charge and

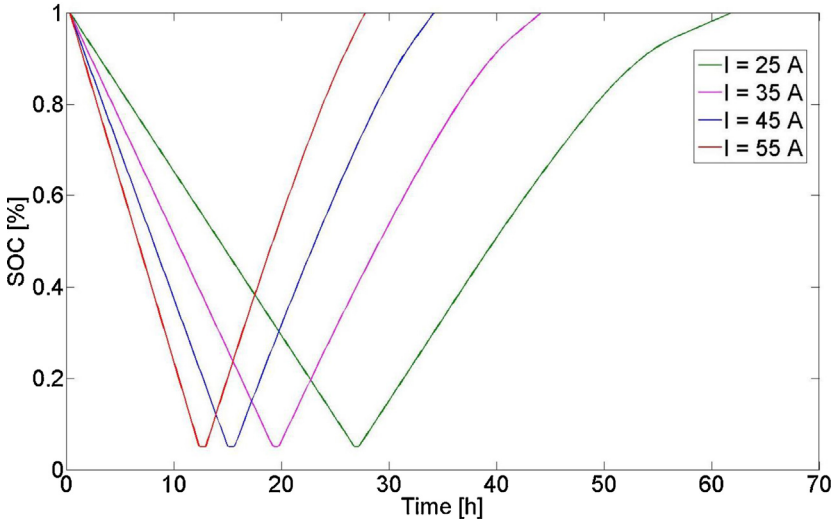

Fig. 3. The influence of the different currents on the battery behavior.

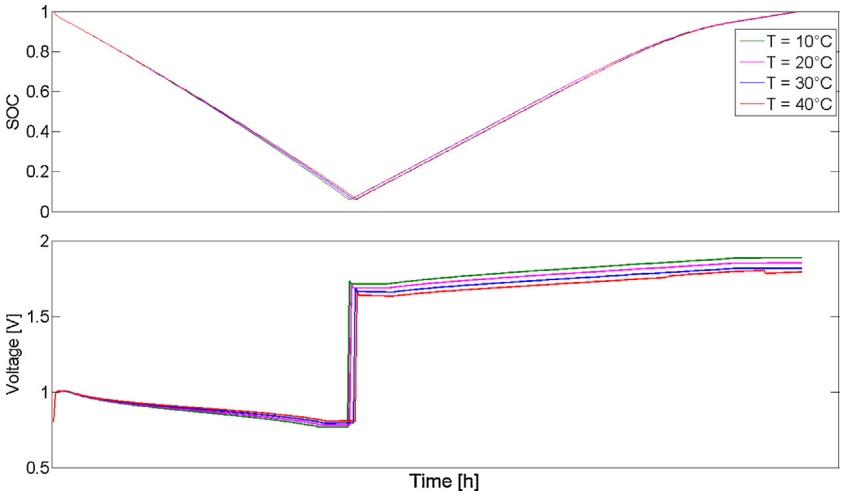

Fig. 4. Battery characteristics over one cycle including the state of charge and voltage at different temperatures.

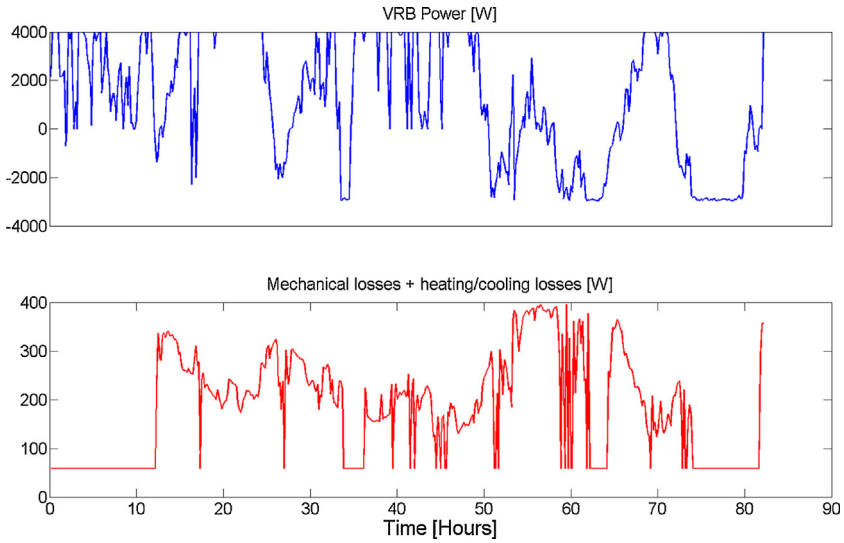

Fig. 5. The VRB system power P_{VRB}, the mechanical losses and the heating/cooling power over the simulation period .The simulation input are taken from [20].

cell voltage at different temperatures during one charging/discharging cycle. The applied current is 35 A.

As it can be seen, the state-of-charge and voltage vary only slightly at different temperatures. The voltage depends on temperature since equilibrium and activation potential are temperature dependent. SOC depends on temperature due to the temperature dependency of the voltage. The state of charge varies only slightly with temperature because it is assumed that within the temperature range of 10 °C to 40 °C no heating and cooling is needed to avoid vanadium precipitation. If heating or cooling is needed, the losses of the battery and thus the SOC vary more widely with temperature. Moreover, the cell voltage curves differ through charging and discharging processes because of the different cell resistances during charging and discharging.

II. Input Parameters for the Simulation

The power profile P_{VRB},which is delivered to the battery system by an external generation unit or discharged from the battery for the external load is shown in Fig. 5. Moreover, the mechanical power losses due to the needed for the pump and the needed power for the heating or cooling the cell are depicted. The profile results from the simulation of a hybrid PV-wind-diesel-battery off-grid system to provide a telecommunication base station with 3 kW electrical power. [18]. The other input parameters are summarized in Table 2. In the simulation, cells with Nafion membranes are assumed.

The concentration overpotential occurs when the rate of the electrochemical reaction is so rapid that “the reactant species do not reach the electrode surface fast enough or that the product species do not leave the electrode fast enough” [4]. Tang et al. examined the link of concentration overpotential and pressure losses to the flow rate in an effort to develop a variable flow rate strategy that can achieve high system efficiency [21]. However, Stirring or agitation, for instance due to the electrolyte flow rate, reduces the thickness of the diffusion layer at the surface of the

Table 4
Diffusion coefficients for the Nafion membrane (temperature dependency is not taken into account for the simulation) [14].

Membrane	k_2 [dm^{-1}]	k_3 [dm^{-1}]	k_4 [dm^{-1}]	k_5 [dm^{-1}]
Nafion	$6.9 \cdot 10^{-7}$	$2.54 \cdot 10^{-7}$	$5.37 \cdot 10^{-7}$	$4.64 \cdot 10^{-7}$

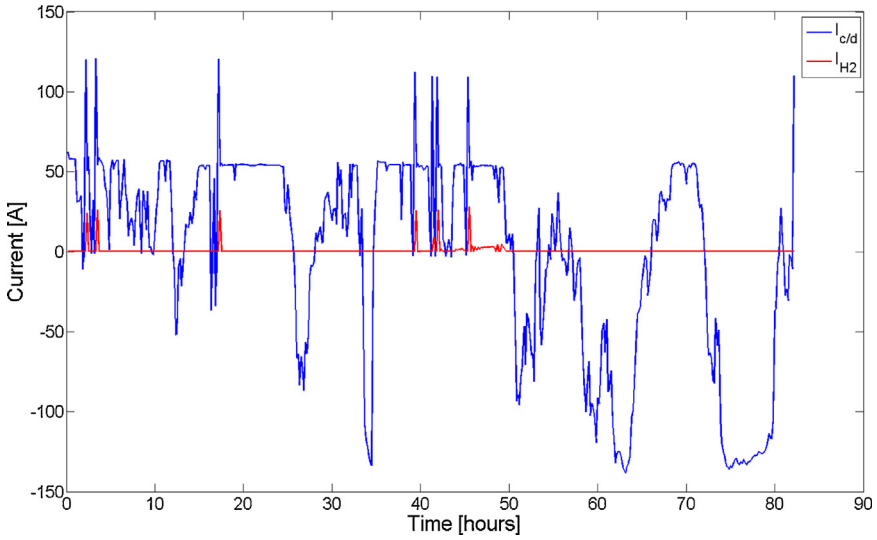

Fig. 6. The charging and discharging currents and the hydrogen evolution current over the simulation period.

electrode and results in a reduction of the concentration overpotential. Thus, it is assumed that the concentration overvoltage is rather small due to the electrolyte flow rate [4].

The parameters for the Vanadium cross-over are summarized in Table 3 and Table 4.

III. Results and Discussion

The battery is simulated over a period of 90 hours. During this time, the battery with 75 kWh is charged and discharged. The corresponding state-of-charge is shown in Fig. 4.

The pumping power losses are between 2% and 6% of the VRB power. This is consistent with estimations of other research groups who expect the pumping losses to have a range of 2–3% of the VRB system power but are higher if the battery is charged at high SOCs, discharged at low SOC or operated at low power (Fig. 5) [22,4].

From Fig. 6 it can be seen that hydrogen evolution only occurs at high SOCs and is quite significant in this period. In the figure only the current for charging and discharging the battery and the hydrogen evolution current are shown because the corrosion current is zero. This can be reached by restricting the cell upper voltage and, therefore, prevent corrosion.

The concentration changes due to vanadium diffusion though the membrane is shown in Fig. 7. It can be seen that the concentration of the different vanadium species change in the range of 10^{-3} mol per second which is consistent with current research.

Fig. 8 shows the surrounding air temperature and the temperature of the stack and the tanks of the Redox-Flow battery. It can be noticed that the temperature in the stack and in the tanks has the same behavior. However, the temperature in the stack is a bit higher than it in the tanks. This can be explained by the cooling effect of the electrolyte mixing in the tanks.

By setting the surrounding temperature to 10 °C, the development of the stack and tank temperature can be seen in Fig. 9. The temperature rises mainly due to the surrounding air temperature and partly because of the heat generation in the stack during charging and discharging the battery (Fig. 10).

4. Conclusion and Outlook

This paper presents a multi-physics model of the all-vanadium redox flow battery. This battery type is a promising candidate for the compensation of fluctuating renewable energy generation, in particular in stand-alone energy generation systems. Until now, none of the existing VRB models was able to accurately predict all

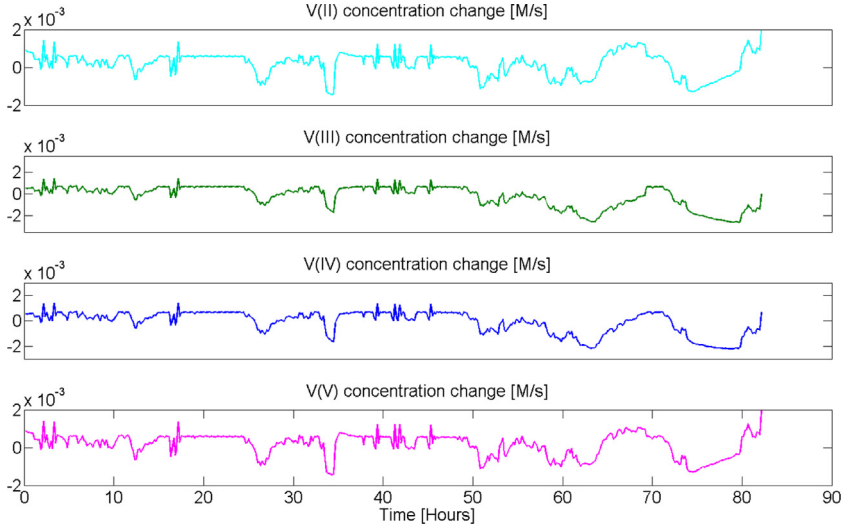

Fig. 7. Concentration change of the different vanadium species due to vanadium cross-over over the simulation period.

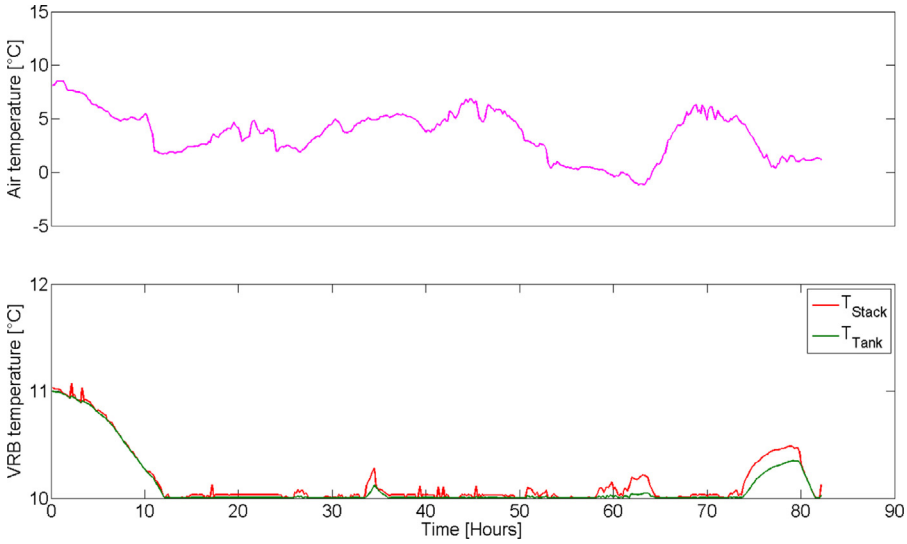

Fig. 8. The surrounding air temperature and the development of stack and tank temperature over the simulation period.

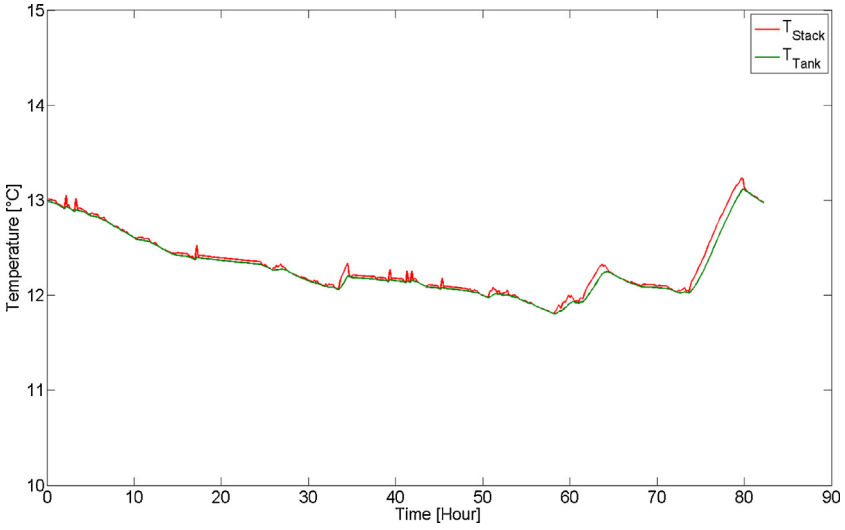

Fig. 9. Development of the stack and tank temperature over the simulation period.

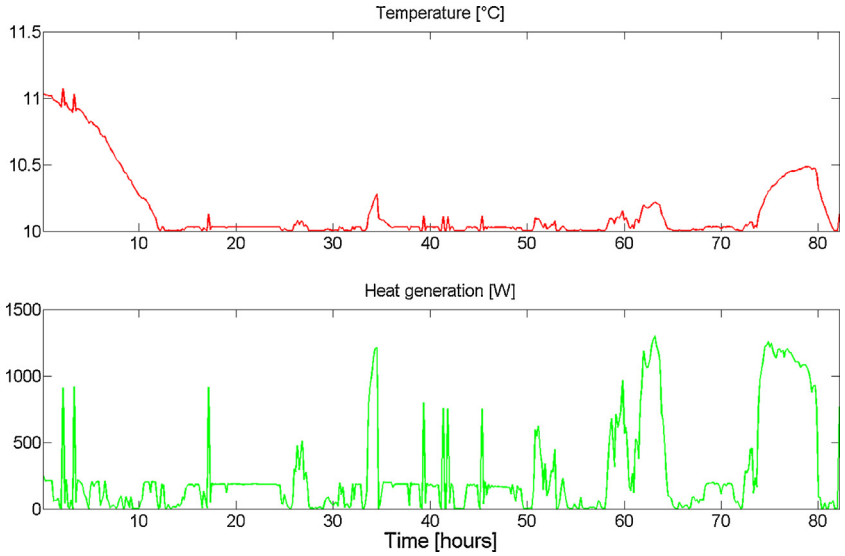

Fig. 10. Heat generation during charging and discharging the battery over the simulation period.

six parameters (SOC, concentration of Vanadium 5, concentration of Vanadium 4, corrosion current, stack Temperature and tank temperature) needed for a new aging model of the VRB, which will be described in the second part of this paper.

The presented model is applicable for VRB systems of different power and capacity ratings, stack and hydraulic circuit designs and electrolyte compositions. A simulation of the presented model shows accurate results which are consistent with current research in this field. Nonetheless, the presented model can be further improved if more experimental data is available on the corrosion and hydrogen evolution within the VRB since the models for these two side reactions are based on experimental data.

References

[1] A. Tang, S. Ting, J. Bao, M. Skyllas-Kazacos, Thermal modelling and simulation of the all-vanadium redox flow battery, Journal of Power Sources 203 (165–176) (2012) 165–176.

[2] J. Chahwan, C. Abbey, G. Joos, VRB Modelling for the Study of Output Terminal Voltages, Internal Losses and Performance. 2007 IEEE Canada Electrical Power Conference.

[3] A. Parasuraman, T.M. Lim, C. Menictas aM. Skyllas-Kazacos, Review of material research and development for vanadium redox flow applications, Electrochimica Acta, pp. 1-14, 2012.

[4] C. Blanc, Modeling of a Vanadium Redox Flow Battery Electricity Storage System, in Thèse numéro 4277 pour l'obtention du grade de docteur ès sciences, École Polytechnique Fédérale de Lausanne, 2009.

[5] C. Blanc, A. Rufer, Multiphysics and Energetic Modeling of a Vanadium Redox Flow Battery, in ICSET 2008: 2008 IEEE International Conference on Sustainable Energy technologies, Singapore, 24–27 November 2008.

[6] C. Blanc, A. Rufer, Optimization of the operating point of a vanadium redox flow battery, in Energy Conversion Congress and Exposition, 2009. ECCE 2009. IEEE, San Jose, California, USA, 20–24 Sept. 2009.

[7] A.Z. Weber, Redox Flow batteries: a review, Journal of Applied Electrochemistry 41, pp. 1137–1164, 2011.

[8] D. You, H. Zhang and J. Chen, A simple model for the vanadium redox battery, Electrochimica Acta 54, no. 6827–6836, 2009.

[9] A.A. Shah, R.S. R. W. R. Tangirala, F. Walsh, A Dynamic Unit Cell Model for the All-Vanadium Flow Battery, Journal of the Electrochemical society 158 (6), pp. A671–A677.

[10] A. Tang, J. Bao, M. Skyllas-Kazacos, Dynamic modelling of the effects of ion diffusion and side reactions on the capacity loss for vanadium redox flow battery, Journal of Power Sources, p. 10737–10747, 2011.

[11] J. Zhao, K. Tseng, M. Skyllas-Kazacos, Extended dynamic model for ion diffusion in all-vanadium redox flow battery including the effects of temperature and bulk electrolyte transfer, Journal of Power Sources, pp. 576–586, 2014.

[12] F. Chen, J. Liu and Y. Chuanwei, Study onHydrogen Evolution Reaction at a Graphite Electrode in the All-Vanadium Redox Flow Battery, International Journal of the Electrochemical Science, Volume 7, pp. 3750–3764, 2012.

[13] H. Liu, Q., Xu, C. Yan, Y. Qiao, Corrosion behavior of a positive graphite electrode in vanadium redox flow battery, Electrochimica Acta 56, pp. 8783-8790, 2011.

[14] J. K. H. L. G. Hovey, Thermodynamics of Sulphuric Acid: Apparent and Partial Molar Heat Capacities and Volumes of Aqueous H2SO4 from 10–55 °C and Calculation of the Second Diccociation Constant to 350°C, Journal od the Chemical Society, Faraday Transactions 86(16), pp. 2831–2839, 1990.

[15] A. M. Sirota, B. K. Mal'tsev and P. Y. Belyakova, Tables of Heat Capacity and Enthalpyof Water and Steam, Teploenergetika, Vol. 10, No. 5, pp. 64–69; available online: http://ntrs.nasa.gov/archive/nasa/casi.ntrs.nasa.gov/19650002671_1965002671 pdf.

[16] B. Bhatt, Stoichiometry, 4th edition, McGraw-Hill Education (India) Pvt Limited, 2004.

[17] L. Brown, T. Holme, Chemistry for Engineering Students, 2nd edition, Belmond, CA, USA. Brooks/Cole, 2010.

[18] D. Skoog, D. West, F. Holler, Analytical chemistry: an introduction, Saunders College Publication, 2000.

[19] R. Badrinarayanan, B., Xiong, J. Zhao, K. Tseng, M. Skyllas-Kazacos, Thermal Hydrolic Behavior and Efficiency Analysis of an All-Vanadium Redox Flow Battery, Journal of Power Sources, pp. 314–324, 2013.

[20] G. Merei, C. Berger, D. Sauer, Optimization of an off-grid hybrid PV-Wind-Diesel system with different battery technologies using genetic algorithm, Solar Energy, pp. 460–473, 2013.

[21] A. Tang, J. Bao, M. Skyllas-Kazacos, Studies on pressure losses and flow rate optimization in vanadium redox flow battery, Journal of Power Sources (2014) 154–162.

[22] R.L. Largent, M. Skylas-Kazacos, J. Chieng, Improved PV system performance using vanadium batteries, Photovoltaic Specialists Conference, 1993., Conference Record of the Twenty Third IEEE, pp. 1119–1124, 10–14 May 1993.